

2024

Quantification of Antiviral Drug Tenofovir (TFV) by Surface-Enhanced Raman Spectroscopy (SERS) Using Cumulative Distribution Functions (CDFs)

Marguerite R. Butler
Old Dominion University, mbutl009@odu.edu


Jana Hrnčirova
Old Dominion University

Meredith Clark
Eastern Virginia Medical School

Sucharita Dutta
Eastern Virginia Medical School

John B. Cooper
Old Dominion University, jcooper@odu.edu

Follow this and additional works at: https://digitalcommons.odu.edu/chemistry_fac_pubs

 Part of the [Analytical, Diagnostic and Therapeutic Techniques and Equipment Commons](#), [Applied Mathematics Commons](#), [Chemicals and Drugs Commons](#), [Immune System Diseases Commons](#), and the [Molecular, Cellular, and Tissue Engineering Commons](#)

Original Publication Citation

Butler, M. R., Hrnčirova, J., Clark, M., Dutta, S., & Cooper, J. B. (2024). Quantification of antiviral drug tenofovir (TVF) by surface-enhanced raman spectroscopy (SERS) using cumulative distribution functions (CDFs). *ACS Omega*, 9(1), 1310-1319. <https://doi.org/10.1021/acsomega.3c07641>

This Article is brought to you for free and open access by the Chemistry & Biochemistry at ODU Digital Commons. It has been accepted for inclusion in Chemistry & Biochemistry Faculty Publications by an authorized administrator of ODU Digital Commons. For more information, please contact digitalcommons@odu.edu.

Quantification of Antiviral Drug Tenofovir (TFV) by Surface-Enhanced Raman Spectroscopy (SERS) Using Cumulative Distribution Functions (CDFs)

Published as part of ACS Omega *virtual special issue* "Celebrating 50 Years of Surface Enhanced Spectroscopy".

Marguerite R. Butler, Jana Hrnčirova, Meredith Clark, Sucharita Dutta, and John B. Cooper*



Cite This: *ACS Omega* 2024, 9, 1310–1319



Read Online

ACCESS |



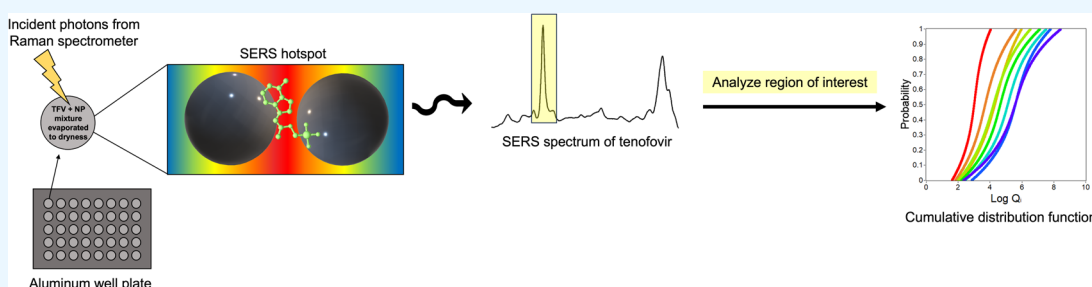
Metrics & More



Article Recommendations



Supporting Information



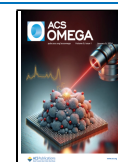
ABSTRACT: Surface-enhanced Raman spectroscopy (SERS) is an ultrasensitive spectroscopic technique that generates signal-enhanced fingerprint vibrational spectra of small molecules. However, without rigorous control of SERS substrate active sites, geometry, surface area, or surface functionality, SERS is notoriously irreproducible, complicating the consistent quantitative analysis of small molecules. While evaporatively prepared samples yield significant SERS enhancement resulting in lower detection limits, the distribution of these enhancements along the SERS surface is inherently stochastic. Acquiring spatially resolved SERS spectra of these dried surfaces, we have shown that this enhancement is governed by a power law as a function of analyte concentration. Consequently, by definition, there is no true mean of SERS enhancement, requiring an alternative approach to achieve reproducible quantitative results. In this study, we introduce a new method of analysis of SERS data using a cumulative distribution function (CDF). The antiviral drug tenofovir (TFV) in an aqueous matrix was quantified down to a clinically relevant concentration of 25 ng/mL using hydroxylamine-reduced silver colloids evaporated to dryness. The data presented in this study provide a rationale for the benefits of combining a novel statistical approach using CDFs with simple and inexpensive experimental techniques to increase the precision, accuracy, and analytical sensitivity of aqueous TFV quantification by SERS. TFV calibration curves generated using CDF analysis showed higher analytical sensitivity (in the form of a normalized calibration curve average slope increase of 0.25) compared to traditional SERS intensity calculations. A second aliquot of nanoparticles and analyte dried on the SERS surface followed by CDF analysis showed further analytical sensitivity with a normalized calibration curve slope increase of 0.23 and decreased variation among replicates represented by an average standard deviation decrease of 0.02 with a second aliquot. The quantitative analysis of SERS data using CDFs presented here shows promise to be a reproducible method for quantitative analysis of SERS data, a significant step toward implementing SERS as an analytical method in clinical and industrial settings.

1. INTRODUCTION

Surface-enhanced Raman spectroscopy (SERS) provides enhanced Raman scattering of molecules through electromagnetic and chemical interactions between a molecule and metal nanostructure.¹ With recorded enhancement factors as high as 10^{14} ,^{2,3} SERS is an exceedingly powerful technique for ultrasensitive detection of low-concentration analytes.⁴ However, this signal enhancement is due to complex factors that, in most cases, are difficult to control,^{5–7} hindering the reproducibility of SERS enhancement. Some of these factors include the background of the SERS surface, morphology of SERS substrates, and stochastic heterogeneity of SERS hotspots

(due to the lack of precise control of the distance between NPs).^{8–11} Consequently, reproducible quantitative and qualitative applications of SERS are inherently difficult to achieve.^{11,12}

Received: October 2, 2023
Revised: November 15, 2023
Accepted: November 27, 2023
Published: December 18, 2023



A general strategy used to improve the reproducibility of SERS enhancement in nonaggregated systems is the application of “Raman reporter” molecules. Generally, these molecules adsorb to both silver and gold and can be nonresonant (i.e., adenine and 4-mercaptobenzoic acid)¹³ or resonant (i.e., rhodamine 6G). Referred to as “extrinsic SERS”, target molecules are measured indirectly through a Raman reporter molecule.¹⁴ In addition to indirect probing, metal nanoparticles can also be modified to have a high specificity for a target molecule. For example, nanoparticles functionalized with an antibody or other ligand can target a specific molecular site,¹⁵ providing a uniform spectral signature of the target analyte and lowering the occurrence of nonspecific binding. While these strategies are often sufficient, the resource investment to implement these methods is greater than the typical surface adsorption of an analyte onto standard silver or gold nanoparticles. Taking this into account, strategies have also been investigated to optimize the reproducibility of SERS enhancement through synthetic improvements to achieve reproducible sizes and geometries.^{16–18} From the perspective of cost and simplicity, perhaps the most effective implementation of SERS for quantitative investigations is the addition of an analyte to a colloidal silver nanoparticle suspension, where appropriate synthetic techniques were taken to yield a narrow distribution of silver sphere diameters.

While this method is useful in several studies,^{19–23} quantitative analysis is limited in signal by an isotherm governing adsorbed and nonadsorbed molecules. To overcome this, an aggregating agent (i.e., NaCl) can be added to the colloidal suspension. To increase SERS enhancement, partially aggregated nanoparticles have the propensity to create more regions of significant electromagnetic enhancement (called SERS “hotspots”) since the space between nanoparticles functions as hotspots.¹⁰ However, this method of induced aggregation lacks reproducibility in terms of aggregate location, density, and composition²⁴ because of the degree of randomness associated with the aggregation process. Colloidal evaporation to dryness is a physical means of aggregation that eliminates the adsorption isotherm in liquid-phase samples as the solvent is evaporated from the surface. As a result, this evaporative method provides significant SERS enhancement relative to liquid-phase samples. Previous studies have demonstrated the advantages of analyzing samples evaporated to dryness, including SERS hotspots concentrated in “coffee-ring” formations of dried analyte–nanoparticle mixtures and detecting nanomolar porphyrin concentrations using immobilized nanoparticles on silanized glass.^{25–27} Additionally, this method provides the ability to increase the analytical sensitivity. Because this method is evaporative, multiple drops can be added, leading to a further concentration enhancement. However, this also results in considerable heterogeneity of SERS hotspots as a function of spatial position, making these enhancements irreproducible.

Tenofovir (TFV) is a nucleoside reverse transcriptase inhibitor (NRTI) that is frequently coadministered with other antiretroviral (ARV) agents for the treatment and prevention of the human immunodeficiency virus (HIV) infection.²⁸ TFV is a main component of the first-line highly active ARV therapy (ART) for the treatment of HIV globally.^{29,30} In combination with emtricitabine, another NRTI, TFV is also used to prevent HIV when taken as a daily pre-exposure prophylaxis (PrEP) regimen.³¹ High adherence to these medication regimens, particularly when prescribed for ART, is important in order for the treatment to remain effective and prevent viral rebound as

well as the emergence of resistant viruses.^{32,33} Detection and quantification of TFV and its metabolites in biological matrices such as plasma and blood cells have been used as objective markers of adherence in clinical trial participants, allowing the identification of those who are compliant with the protocol.^{33–36} This, in turn, is important to assessing the true effect of the experimental intervention. Previous work in our laboratory has shown that while this quantification was possible using the entire SERS surface generated by the evaporative process described above, the analytical sensitivity was enhanced by selecting SERS spectra corresponding to high signal-to-noise ratio (S/N) as a function of spatial position using a scanning Raman system to acquire spatially resolved spectra. Furthermore, our previous work reported the added benefit of using a colloidal evaporative process: additional colloidal depositions could be made onto a surface and evaporated, effectively increasing the prevalence of SERS hotspots, and further enhancing analytical sensitivity.³⁷

These investigations have shown that there is a large distribution of SERS enhancements across the surface ranging from no signal enhancement to extreme enhancement from SERS hotspots. Histograms of spatially resolved SERS spectra illustrate a power law for SERS enhancement such that there are more weak SERS signals than strong SERS signals. This can be attributed to many factors (i.e., nanoparticle arrangement and proximity, packing density, and molecular adsorption geometry) that are influenced by the stochastic colloidal evaporation process. Because SERS enhancement for these samples follows a power law, there is no true mean spectral intensity, making the mean SERS spectrum, by definition, irreproducible. Cumulative distribution functions (CDFs) are useful in modeling data governed by a power law, where traditional normal distributions do not apply. Generally, CDFs illustrate the probability that a given variable will take on a value less than or equal to a specific point, showing cumulative probabilities across a range of values. Unlike a probability density function, which shows the probability of specific outcomes, a CDF accumulates these probabilities in an ascending fashion. Therefore, for increasing x -values across a CDF, the line ascends, reflecting the growing total (accumulating) probability of encountering a value less than or equal to that point. CDFs have been previously utilized in a few applications, including mass spectrometry³⁸ and genomics.³⁹

In this work, spatially resolved Raman spectra acquired from solid SERS surfaces prepared through an evaporative process of Ag colloids containing TFV molecules are analyzed using CDFs. Using these CDFs, calibration curves of aqueous TFV with improved analytical sensitivity and precision (relative to S/N selection and spectral averaging) are generated. The analysis of SERS data using CDFs presented in this study shows promise for being a reproducible method for the quantitative analysis of evaporated samples. The methods presented in this study maintain the benefit of analyte concentration through the evaporative process yet also minimize the effect of SERS enhancement irreproducibility (due to forced aggregation) by modeling the SERS enhancement as a CDF. Overall, these findings represent a significant step toward implementing SERS as an analytical method in clinical and industrial settings. The use of CDFs to analyze and quantify SERS spectral data has not been demonstrated before this investigation.

2. EXPERIMENTAL SECTION

Ag colloidal nanoparticles (CNPs) were prepared by the reduction of silver nitrate (Sigma-Aldrich) with hydroxylamine

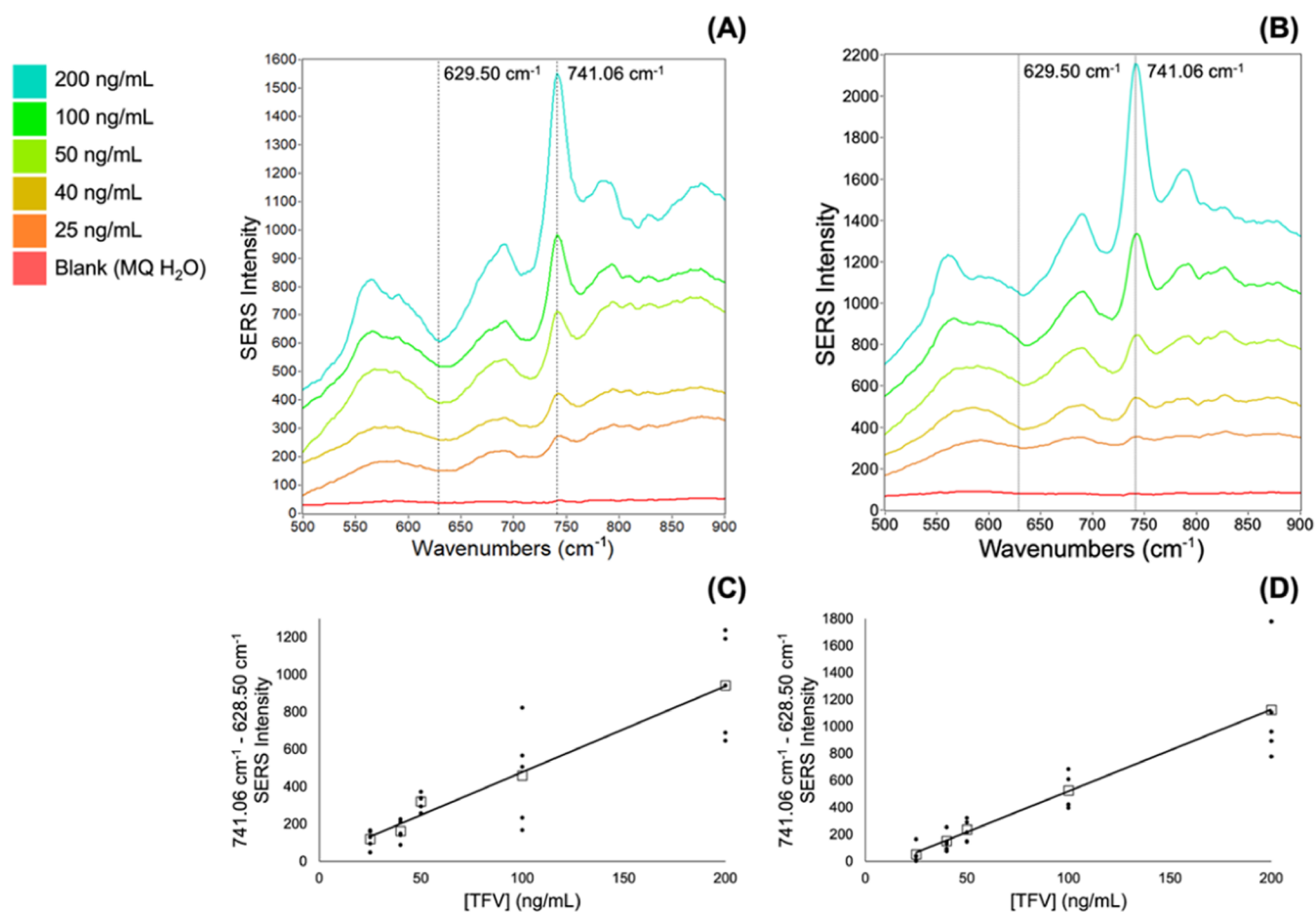


Figure 1. Average SERS spectra of the top 100 Q_i ranked spectra out of 9030 acquired spectra for each TFV concentration. (A) Single-deposition data set. (B) Double-deposition data set. Calibration curves of TFV where the difference between SERS intensities at 628.50 and 741.06 cm^{-1} was plotted as a function of the TFV concentration. (C) Single-deposition data set. (D) Double-deposition data set. Hollow squares in the calibration curves represent the average of all replicates, and filled circles represent each replicate. A 7-point Savitzky–Golay smooth function was applied to all spectra and offset for clarity. See Figure S2 for the full SERS spectra.

hydrochloride (Sigma) as described by Leopold and Lendl.⁴⁰ Briefly, 300 μL of 1 M NaOH (Fisher Chemical) was added to 90 mL of 1.6×10^{-3} M hydroxylamine hydrochloride. The mixture was stirred continuously at 360 rpm as 10 mL of 1×10^{-2} M silver nitrate was added dropwise. The UV–visible spectra of these syntheses are shown in Figure S1. The solution was stirred for an additional 45 min. Aqueous TFV calibration standards were prepared using ultrapure Milli-Q (MQ) (MilliporeSigma) water and powder TFV provided by CONRAD at Eastern Virginia Medical School (manufactured by Gilead Alberta ULC). An aluminum well plate (certified 1100 aluminum) containing 40 machined wells in an 8×5 array was used as the SERS surface. Reaction mixtures consisting of equal volumes of the CNP suspension and TFV standards were prepared in separate microcentrifuge tubes and briefly vortexed before deposition on the aluminum well plate. Each TFV concentration had five replicates, and the gradient consisted of seven TFV concentrations in the range of 500–25 ng/mL, and a matrix blank of MQ H_2O . A 20 μL aliquot of these eight reaction mixtures were each deposited into five aluminum wells and evaporated to dryness in a chemical hood before acquiring spectra. For the TFV double-deposition experiment, this mixture, deposition, and evaporation process were repeated for one additional reaction mixture aliquot of 20 μL in each well. A computerized XY stage (ThorLabs) holding the Raman

spectrometer⁴¹ was used for spectral acquisition of each replicate on the aluminum well plate. A Wasatch Photonics 785 nm excitation laser was used for the Raman measurements. This excitation wavelength is generally accepted for maximizing the Raman signal because it minimizes fluorescence interference and maximizes Raman scattering compared to shorter or longer excitation wavelengths. The charge-coupled device (CCD) used has 1024 pixels, covering a calibrated spectral range of 269.89 to 2005.41 wavenumbers (cm^{-1}). The average effective resolution across the spectral range is approximately 17 cm^{-1} . The results presented are based on the calibrated wavenumber of each discrete pixel, which is reported by the manufacturer to two decimal places. A raster scan pattern was used for acquisition. An integration time of 800 ms and 15 mW of laser power was used.

3. RESULTS AND DISCUSSION

3.1. Calibrations Using Spectra Averaging and SERS Intensities. As shown in our previously published studies,³⁷ calculating the difference between the SERS intensity of a peak and baseline as a function of analyte concentration yields a linear calibration curve. We also established the importance of spectral selection based on a figure-of-merit (FOM) quality index (Q_i) due to the profound effect of analytical sensitivity (shown by the calibration curve slope) when including spectra with low Q_i values (corresponding to poor S/N). Shown in Figure 1, the top

Table 1. Linear Regression Equations and Correlation Coefficients for Calibration Curves Generated Using SERS Intensities Shown in Figure 1C,1D for TFV Data Sets Single and Double Deposition, Respectively

TFV data set	linear regression ($y = mx + b$)	correlation coefficient (R^2)
single deposition	$y = 4.6098x + 18.651$	0.9834
double deposition	$y = 6.0711x - 85.492$	0.9991

20 spectra from each replicate for all concentrations corresponding to the highest Q_i of the 741 cm^{-1} peak were averaged, resulting in one spectrum for every concentration consisting of 100 spectra. The difference between the SERS intensity at 741.06 and 628.50 cm^{-1} was then plotted as a function of TFV concentration (Figure 1).

As shown in Figure 1, there is a linear change in this SERS intensity difference with TFV concentration. Furthermore, the linear slope for the calibration curve from the TFV double-deposition data set is greater than the single-deposition data set

(see Table 1), consistent with increased analytical sensitivity from an additional colloidal aliquot. However, it is important to recognize the variability of the SERS intensity across the individual replicates. Evaporating our samples to dryness forces the aggregation of NPs and adsorption of TFV on the aluminum surface, concentrating the analyte. However, evaporating to dryness also results in a nonuniform conformation of analyte molecules adsorbed to the SERS substrate, producing a heterogeneous surface and stochastic SERS hotspots. This is illustrated in Figure 1 by the large spread of replicate SERS intensity differences (shown by filled circles), especially in the single-deposition data set (Figure 1A,1C).

We acquired spatially resolved SERS spectra for each replicate represented by a well on the aluminum plate in a raster pattern as shown in Figure 2. When analyzing the spectra acquired at all spatial positions for a single replicate, it is apparent that there is a vast distribution of spectra in terms of the analyte signal intensity. Figure 2 shows all acquired spectra for a single replicate of 200 ng/mL TFV from both the single- and double-

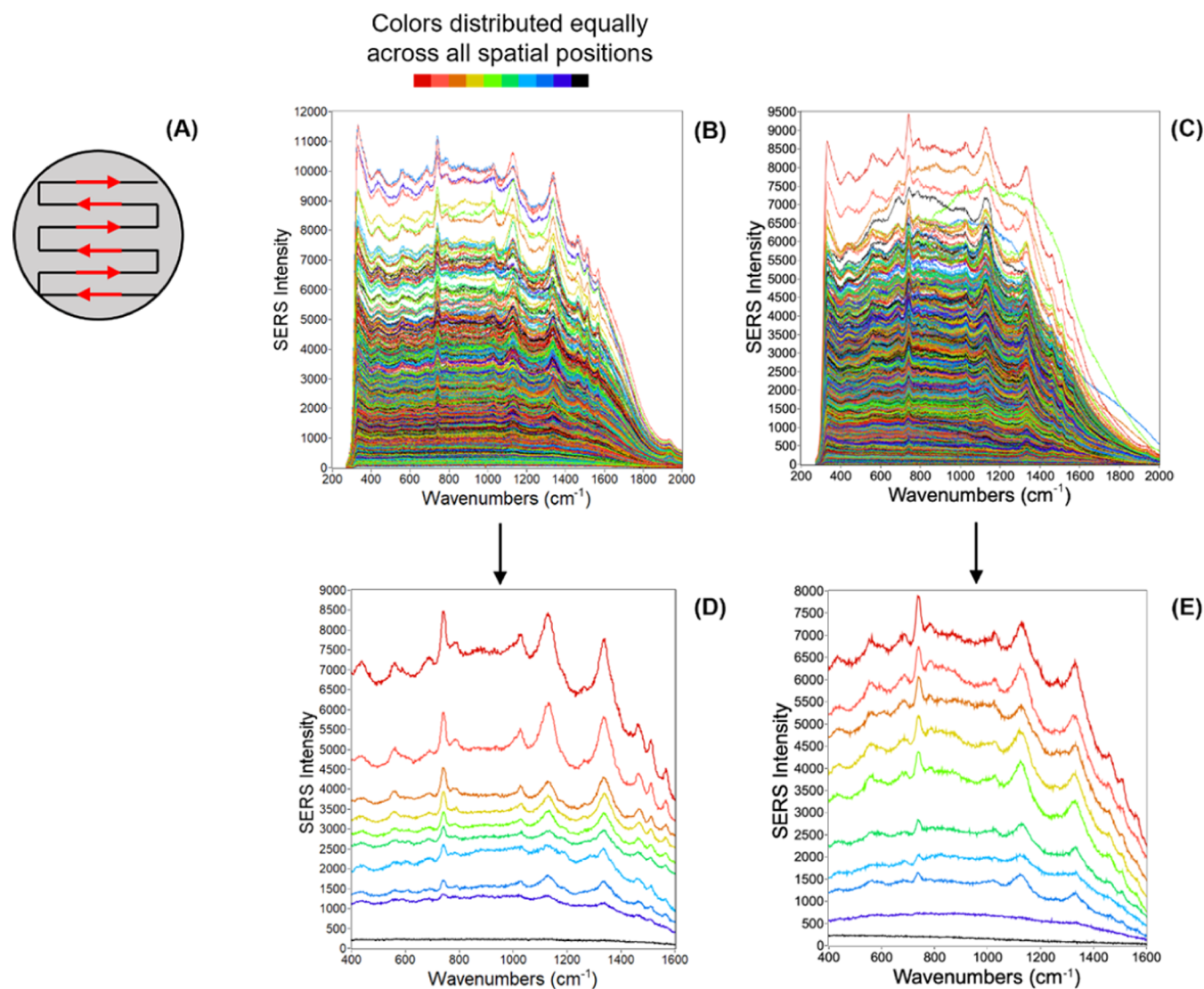


Figure 2. (A) Raster scan pattern used for acquiring spatially resolved spectra of the solid SERS surfaces in each aluminum well. All spectra acquired from a single well containing 200 ng/mL TFV. (B) Single-deposition data set. (C) Double-deposition data set. Selected individual spectra were from 200 ng/mL TFV replicates. (D) Single-deposition replicate. (E) Double-deposition replicate. Ten colors distributed evenly across all spatial positions were used to color all spectra. Individual spectra were offset for clarity.

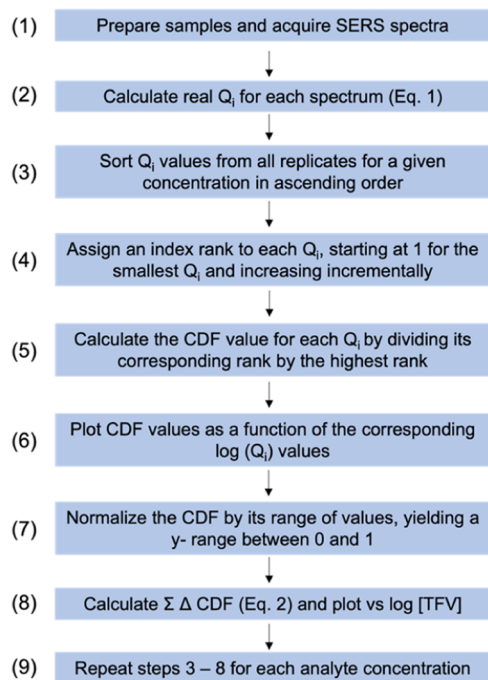


Figure 3. Process diagram of using CDFs for quantitative analysis of SERS data for TFV.

deposition data sets, colored using 10 different colors evenly distributed across all spatial positions. Pulling select spectra from all spatial positions (Figure 2) exemplifies this distribution of the S/N for acquired SERS spectra. Consequently, there is not a true mean that is representative of the entire data population, making calibration curves of raw SERS intensities (shown in Figure 1) irreproducible across different data sets, consistent with a relationship governed by a power law. This can be illustrated by histograms showing the Q_i distribution across each TFV concentration (Figures S3 and S4).

3.2. Calibrations Using Cumulative Distribution Functions (CDFs). For the acquired spatially resolved spectra, Q_i was calculated for each spectrum as shown in eq 1:

$$Q_i = \left(\prod_{k=1}^t \left\{ \frac{1}{2n+1} \left[\sum_{j=p-n}^{p+n} I_j - \sum_{j=b_1-n}^{b_1+n} I_j \right] \times \left(\sum_{j=p-n}^{p+n} I_j - \sum_{j=b_2-n}^{b_2+n} I_j \right) \right\} \right)^{1/t} \quad (1)$$

Any Q_i value less than 0 was defined as $Q_i = 0$.

Briefly, the sum of SERS intensities at points I_j was calculated to determine the average intensity about each peak p and baselines b_1 and b_2 (+) and (−) n number of points. This summation was then raised to the inverse power of the total number of peaks used for Q_i , t . The distribution of Q_i 's assigned

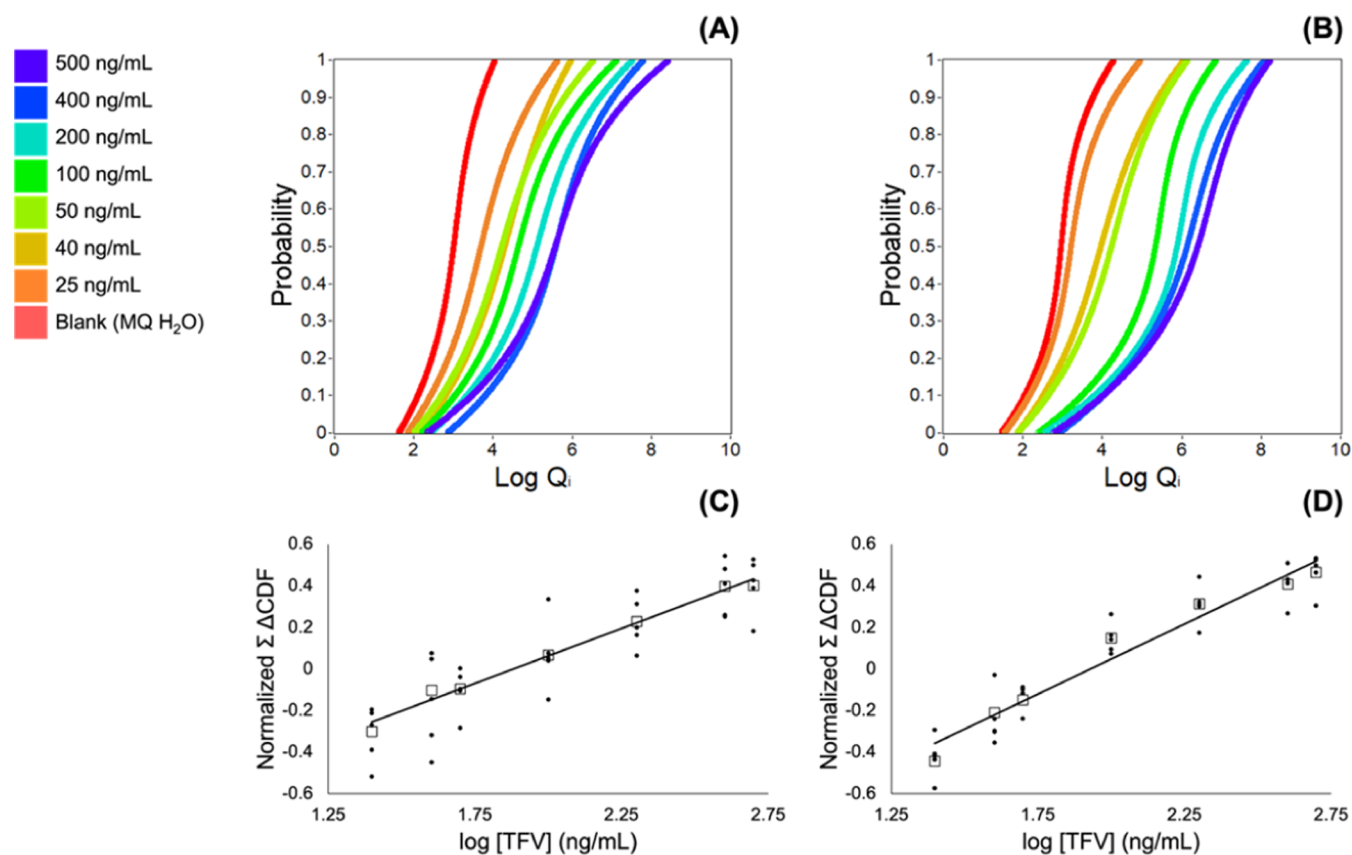


Figure 4. CDF calibrations of both TFV data sets using the entire probability range of the CDF (0–1). Model CDFs of each TFV concentration. (A) Single-deposition data set. (B) Double-deposition data set. $\Sigma \Delta$ CDF plotted as a function of the logarithm of TFV concentration. (C) Single-deposition data set. (D) Double-deposition data set. Vertical axes were range scaled for clarity. Hollow squares represent model CDFs, and filled circles represent replicate CDFs.

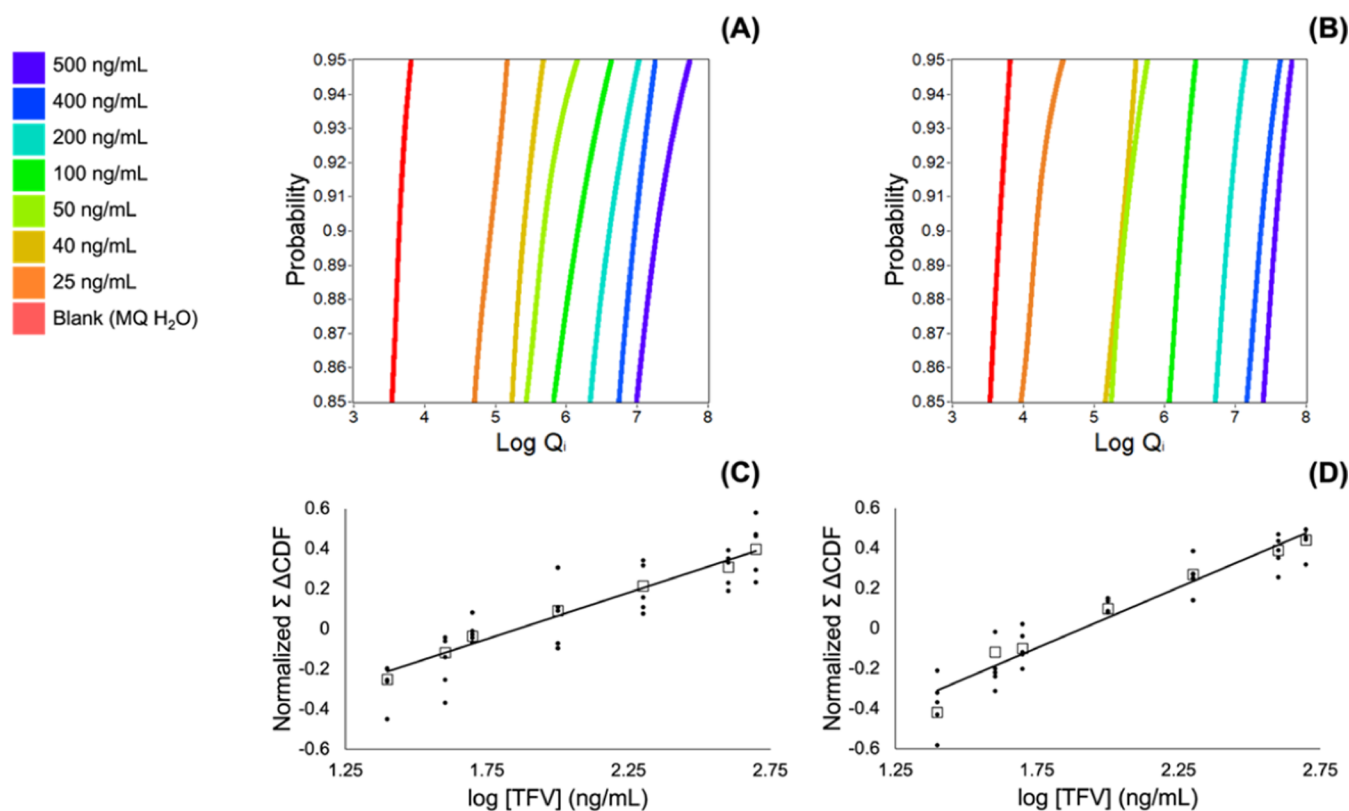


Figure 5. CDF calibrations of both TFV data sets using the CDF probability range 0.85–0.95. Model CDFs of each TFV concentration. (A) Single-deposition data set. (B) Double-deposition data set. $\sum \Delta\text{CDF}$ plotted as a function of the logarithm of TFV concentration. (C) Single-deposition data set. (D) Double-deposition data set. Vertical axes were range scaled for clarity. Hollow squares represent model CDFs, and filled circles represent replicate CDFs.

Table 2. Linear Regression Equations and Correlation Coefficients for $\sum \Delta\text{CDF}$ Calibration Curves Shown in Figures 4 and 5

figure	TFV data set	CDF probability region	linear regression ($y = mx + b$)	R^2
4B	single	0–1	$y = 0.5283x - 0.9939$	0.9875
4D	double	0–1	$y = 0.6732x - 1.299$	0.9635
5B	single	0.85–0.95	$y = 0.4622x - 0.8582$	0.9850
5D	double	0.85–0.95	$y = 0.6032x - 1.1525$	0.9611

to each spectrum was then used to generate a CDF. The CDF provides comprehensive information about the distribution of Q_i values (a variable calculated based on a spectral region of interest) across concentrations. The probability that a Q_i takes on a value less than or equal to a specific value (in this case, the maximum Q_i) can be determined. Overall, the true CDF shows the cumulative probabilities of all possible values of Q_i for a given analyte concentration. By evaluating the CDF at a particular Q_i , the probability of observing a Q_i value less than or equal to that of Q_i can be determined.

To calculate a CDF for each TFV concentration replicate using Q_i values, the nonzero values were first sorted and ranked by assigning an arbitrary index starting at 1 to the lowest Q_i value and increasing incrementally. The “probability” (in this case the y -axis) for each Q_i in the CDF was calculated by dividing its rank by the highest rank (highest index value). This was calculated for all ranks. All of these quotients were then plotted as a function of the logarithmic value of their corresponding Q_i . This generated a total of five CDFs for each concentration, corresponding to the five solid SERS surfaces created (evaporated mixture of Ag

colloidal suspension and aqueous TFV) for each concentration. To generate a “model” CDF using all Q_i values corresponding to a TFV concentration, all nonzero Q_i values were added to a single array. The calculations described above for a replicate CDF were then performed for this array, generating a single “model” CDF consisting of Q_i data from all replicates for each concentration. All subsequent calculations and results discussed in the preceding sections are from model CDFs.

By taking the point difference between two CDF curves at the same probability, we can calculate an error of the $\log(Q_i)$ value. The value of this error starts at 0 for the same CDF at the same concentration but progressively increases as the concentration difference between the CDFs increases (Figures 4 and 5). This allows a calibration curve to be created using the model CDFs by summing the errors for each concentration (eq 2) calculated from all of the populated probability points of the CDFs. See Figure 3 for a process diagram summarizing these steps.

$$n = \sum \Delta\text{CDF} = \sum_{x=n}^{x=n+7} [\text{CDF}(n) - \text{CDF}(x)] \quad (2)$$

where n is the concentration index, and the CDF difference is pointwise.

Because the errors were pointwise differences, 500 fit points (calculated from a third-order polynomial equation generated for each model CDF) spaced evenly across the CDF probability were used to equally populate each model CDF for $\sum \Delta\text{CDF}$ calculations (Figures 4 and 5). Cumulative distribution plots showing only the raw CDF values for each TFV concentration are shown in Figure S5. Although in all instances the CDFs

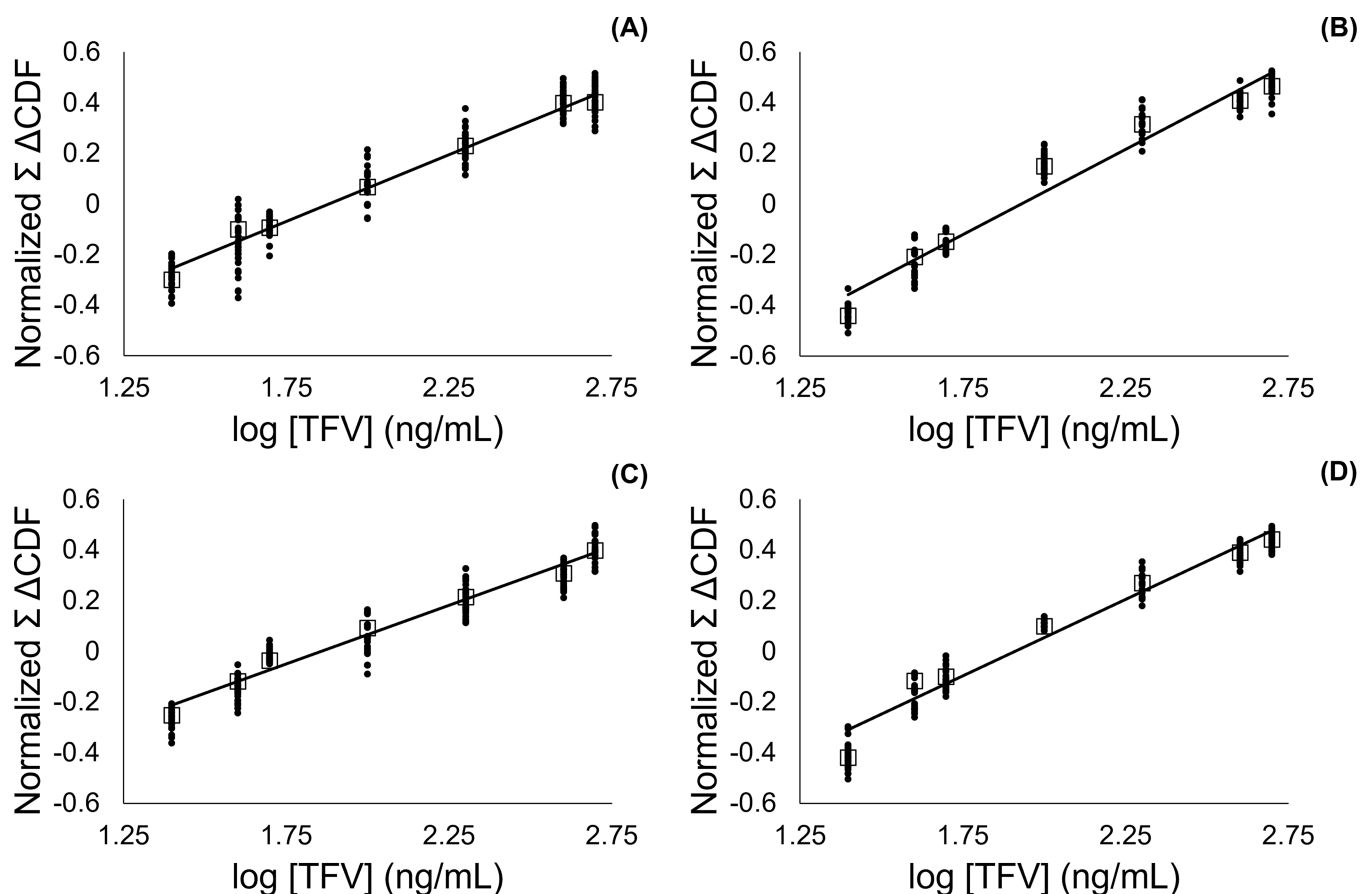


Figure 6. $\Sigma \Delta$ CDF calibration curves showing the spread of replicate $\Sigma \Delta$ CDF data points (filled circles) relative to model CDF $\Sigma \Delta$ CDF data points (hollow squares) where each replicate CDF is comprised of Q_i data from four replicates concentration using probability range 0–1 for (A) single-deposition data set and (B) double-deposition data set, and probability range 0.85–0.95 for (C) single-deposition data set and (D) double-deposition data set.

correspond to a probability range (y -axis) from 0 to 1 (Figure 4), observation makes it clear that CDFs defined using a narrower range of probabilities (e.g., 0.85–0.95) provide greater differences between the model CDFs and would thus be more useful in calibration construction (Figure 5).

As shown in Figures 4, 5, and Table 2, the linear slopes of the calibration curves of the double-deposition data set were greater than the slopes of calibration curves of the single-deposition data set, indicating greater analytical sensitivity from an additional colloidal aliquot. Interestingly, the linear slopes of both data sets using a smaller probability range of the CDF were less than the slopes of both data sets using the entire probability range. Presumably, this could be the result of using a larger window of data that was poorly fitted by a low-order polynomial at both extreme ends of the probability range (where the slope of the CDF curve is low). However, using a small probability range that corresponds to steep and consistent slopes of the CDFs makes a low-order polynomial function a great option for accurately fitting the data.

An analysis utilizing the central limit theorem (CLT) (Figure 6) was performed on the four calibration curves shown in Figures 4 and 5. A key point of the CLT states that for a sufficiently large sample size, the distribution of random variables (in this case, replicates generated from random combinations of 4 out of the 5 concentration replicates) will be normally distributed about the mean (in this case, the $\Sigma \Delta$ CDF of each model CDF).

Exemplified by the data shown in Figure 6, an important aspect of CDF analysis is the actual number of real Q_i values (defined as a positive nonzero integer in eq 1) available to be factored in the model CDFs for $\Sigma \Delta$ CDF calculations. To be expected, the number of spectra with nonzero Q_i values decreases with decreasing TFV concentration for both data sets. Based on the data shown in Figure 6, additional sampling of the SERS surfaces (i.e., smaller lines of separation in the raster scan pattern) would be needed for increased precision. This is apparent in Figure 6 such that more Q_i values comprising each replicate (shown by the filled circles) provide a drastically smaller spread of replicate $\Sigma \Delta$ CDF relative to model $\Sigma \Delta$ CDF (compared to Figures 4 and 5). With increased sampling, a convergence to the true CDF would be possible for samples that have sparse nonzero Q_i s, increasing the precision of the $\Sigma \Delta$ CDF calibration curves.

3.3. Comparison of Both Quantitative Methods. To compare both quantitative methods, a normalization eq (eq 3) was applied to both quantitative data sets (SERS intensity averaging and $\Sigma \Delta$ CDF) to allow direct comparison between calibration curves shown in Figure 7.

$$\text{normalized response } i = \frac{[y_i - \min(y)]}{[\max(y) - \min(y)]} \quad (3)$$

Briefly, the normalized response of the i th data point was calculated by subtracting the minimum response of the data set

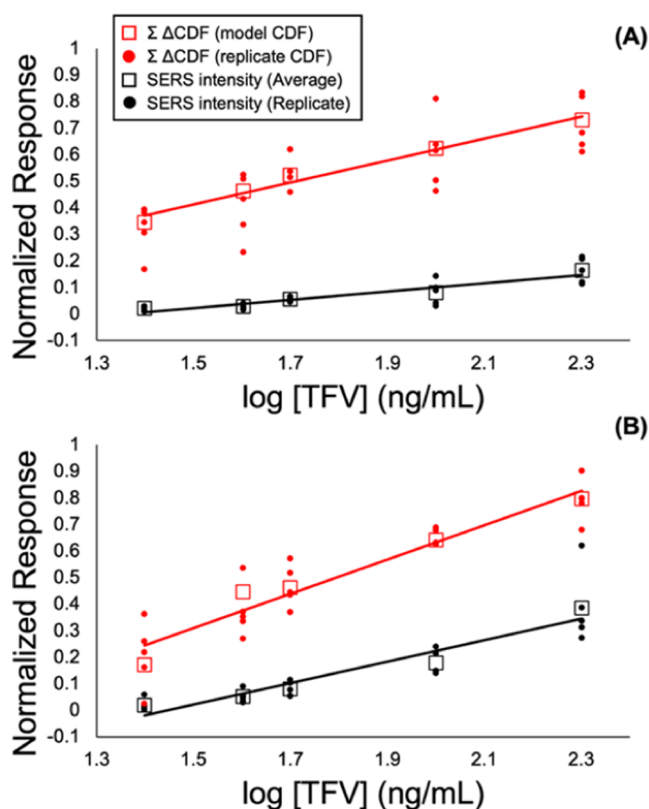


Figure 7. Comparison of data analysis methods SERS intensity averaging (black) and CDF analysis ($\Sigma \Delta\text{CDF}$) (red) in the probability range 0.85–0.95. (A) Single-deposition data set. (B) Double-deposition data set. Responses from both analysis methods were normalized on a 0–1 scale (eq 3). TFV concentrations 25 ng/mL–200 ng/mL are shown and were used for linear regression calculations (Table 3).

Table 3. Linear Regression Equations and Correlation Coefficients for Data Shown in Figure 7

data set	data analysis method	linear regression equation ($y = mx + b$)	R^2
single	$\Sigma \Delta\text{CDF}$	$y = 0.4130x - 0.2072$	0.9805
double	$\Sigma \Delta\text{CDF}$	$y = 0.6453x - 0.6577$	0.9474
single	SERS intensity averaging	$y = 0.1553x - 0.211$	0.9244
double	SERS intensity averaging	$y = 0.4036x - 0.5835$	0.9334

from i th data point then divided by the difference between the maximum and minimum response of the data set.

As shown in Figure 7 and Table 3, CDF analysis of both data sets in the probability range 0.85 to 0.95 (Figure 5 and Table 2) yielded calibration curves with higher analytical sensitivity than calibration curves generated by averaging SERS intensity (Figure 1 and Table 1) of spectra with the highest S/N (shown by the linear slope values). Based on these data, analysis of SERS data using the CDF approach presented provides improved discrimination of TFV concentrations down to 25 ng/mL relative to the traditional method of subtracting the SERS intensity from a baseline region from the intensity of a peak. Additionally, an increase in analytical sensitivity provided by analyzing double-deposition SERS data by CDFs showed a smaller spread among replicates relative to the single-deposition data set, consistent with improved precision of quantitation. The

average difference between the standard deviation of $\Sigma \Delta\text{CDF}$ values for each concentration between the single- and double-deposition data set was 0.02 (Table S1), further demonstrating the improved precision of quantitation with an additional aliquot.

4. CONCLUSIONS

In conclusion, this study addressed the inherent challenges associated with quantitative analysis by SERS. While incredibly sensitive, SERS has long suffered from issues of poor reproducibility, particularly in the context of quantitative analysis due to highly variable SERS enhancement across a surface. This research sheds light on the stochastic nature of SERS enhancement as a function of analyte concentration, revealing a power-law relationship. To overcome this, we innovatively employed CDFs as a statistical approach to quantitatively analyze spatially resolved SERS spectral data. The application of this method to the quantification of the antiviral drug TFV in an aqueous matrix has yielded remarkable results. TFV could be reliably quantified at clinically relevant concentrations (down to 25 ng/mL), a significant achievement that paves the way for the development of a robust analytical assay. Moreover, the calibration curves generated using CDFs demonstrated higher analytical sensitivity and reduced variation among replicates when compared to traditional SERS intensity calculations. The addition of a second aliquot of nanoparticles and analyte dried on the SERS surface further enhanced the analytical sensitivity and minimized replicate variation. Overall, this research opens promising avenues for SERS to be adopted as a robust analytical technique in clinical and industrial settings. By combining innovative statistical analysis with cost-effective experimental approaches, our work has significantly improved the precision and analytical sensitivity of aqueous TFV quantification by SERS. This marks a substantial step forward in harnessing the full potential of SERS for practical applications, offering a reliable method for quantitative analysis that holds great promise for various fields.

■ ASSOCIATED CONTENT

Supporting Information

The Supporting Information is available free of charge at <https://pubs.acs.org/doi/10.1021/acsomega.3c07641>.

UV–vis spectra of nanoparticles (Figure S1), SERS spectra from both deposition data sets showing the entire spectral range (Figure S2), histograms of the Q_i distribution for all acquired spectra for both deposition data sets (Figures S3 and S4), unfitted CDFs for both deposition data sets (Figure S5), and standard deviation of $\Sigma \Delta\text{CDF}$ values for each TFV concentration in both data sets (Table S1) (PDF)

■ AUTHOR INFORMATION

Corresponding Author

John B. Cooper – Department of Chemistry and Biochemistry, Old Dominion University, Norfolk, Virginia 23529, United States; orcid.org/0000-0001-9167-9589; Email: jcooper@odu.edu

Authors

Marguerite R. Butler – Department of Chemistry and Biochemistry, Old Dominion University, Norfolk, Virginia 23529, United States; orcid.org/0009-0006-5828-8838

Jana Hrcirova – Department of Chemistry and Biochemistry, Old Dominion University, Norfolk, Virginia 23529, United States; Department of Physical and Macromolecular Chemistry, Charles University, Hlavova 2030, Czech Republic

Meredith Clark – Department of Obstetrics and Gynecology, Eastern Virginia Medical School, Norfolk, Virginia 23507, United States

Sucharita Dutta – Department of Obstetrics and Gynecology, Eastern Virginia Medical School, Norfolk, Virginia 23507, United States

Complete contact information is available at:

<https://pubs.acs.org/10.1021/acsomega.3c07641>

Funding

This work was funded by subaward ENS-20-001 from CONRAD/EVMS under Project Engage, a cooperative agreement (7200AA20CA00030) between the U.S. Agency for International Development (USAID) and EVMS funded by U.S. President's Emergency Plan for AIDS Relief (PEPFAR). The views of the authors do not necessarily reflect those of the funding agency, PEPFAR, or the U.S. Government.

Notes

The authors declare no competing financial interest.

ACKNOWLEDGMENTS

The authors would like to extend their gratitude to the United States Agency for International Development (USAID) for the funding provided to make this research possible. Additionally, the first author would like to acknowledge CONRAD members Terry Jacot and Gustavo Doncel for collaboration on ongoing projects pertaining to this research.

REFERENCES

- (1) Jensen, L.; Aikens, C. M.; Schatz, G. C. Electronic structure methods for studying surface-enhanced Raman scattering. *Chem. Soc. Rev.* **2008**, *37* (5), 1061–1073.
- (2) Kneipp, K.; Wang, Y.; Kneipp, H.; et al. Single Molecule Detection Using Surface-Enhanced Raman Scattering (SERS). *Phys. Rev. Lett.* **1997**, *78* (9), 1667–1670.
- (3) Nie, S.; Emory, S. R. Probing Single Molecules and Single Nanoparticles by Surface-Enhanced Raman Scattering. *Science* **1997**, *275* (5303), 1102–1106.
- (4) Sharma, B.; Frontiera, R. R.; Henry, A. I.; et al. SERS: Materials, applications, and the future. *Mater. Today* **2012**, *15* (1), 16–25.
- (5) Aroca, R. F.; Rodríguez-Llorente, S. *Surface Enhanced Vibrational Spectroscopy*; Wiley, 2006.
- (6) Qiu, Y.; Kuang, C.; Liu, X.; et al. Single-Molecule Surface-Enhanced Raman Spectroscopy. *Sensors* **2022**, *22* (13), 4889.
- (7) Bell, S. E. J.; Sirimuthu, N. M. S. Quantitative surface-enhanced Raman spectroscopy. *Chem. Soc. Rev.* **2008**, *37* (5), 1012–1024.
- (8) Saviello, D.; Trabace, M.; Alyami, A.; et al. Raman Spectroscopy and Surface Enhanced Raman Scattering (SERS) for the Analysis of Blue and Black Writing Inks: Identification of Dye Content and Degradation Processes. *Front. Chem.* **2019**, *7*, No. 727, DOI: 10.3389/fchem.2019.00727.
- (9) Puente, C.; Sánchez-Domínguez, M.; Brosseau, C. L.; et al. Silver-chitosan and gold-chitosan substrates for surface-enhanced Raman spectroscopy (SERS): Effect of nanoparticle morphology on SERS performance. *Mater. Chem. Phys.* **2021**, *260*, No. 124107.
- (10) Shiohara, A.; Wang, Y.; Liz-Marzán, L. M. Recent approaches toward creation of hot spots for SERS detection. *J. Photochem. Photobiol., C* **2014**, *21*, 2–25.
- (11) Pérez-Jiménez, A. I.; Lyu, D.; Lu, Z.; et al. Surface-enhanced Raman spectroscopy: benefits, trade-offs and future developments. *Chem. Sci.* **2020**, *11* (18), 4563–4577.
- (12) Fornasaro, S.; Alsamad, F.; Baia, M.; et al. Surface Enhanced Raman Spectroscopy for Quantitative Analysis: Results of a Large-Scale European Multi-Instrument Interlaboratory Study. *Anal. Chem.* **2020**, *92* (5), 4053–4064.
- (13) Bell, S. E. J.; Charron, G.; Cortés, E.; et al. Towards Reliable and Quantitative Surface-Enhanced Raman Scattering (SERS): From Key Parameters to Good Analytical Practice. *Angew. Chem., Int. Ed.* **2020**, *59* (14), 5454–5462.
- (14) Magdy, M. A. Conceptual Overview of Surface-Enhanced Raman Scattering (SERS). *Plasmonics* **2023**, *18* (2), 803–809.
- (15) Israelsen, N. D.; Hanson, C.; Vargis, E. Nanoparticle Properties and Synthesis Effects on Surface-Enhanced Raman Scattering Enhancement Factor: An Introduction. *Sci. World J.* **2015**, *2015*, No. 124582.
- (16) Luechinger, N. A.; Athanassiou, E. K.; Stark, W. J. Graphene-stabilized copper nanoparticles as an air-stable substitute for silver and gold in low-cost ink-jet printable electronics. *Nanotechnology* **2008**, *19* (44), No. 445201.
- (17) Xue, M.; Zhang, Z.; Zhu, N.; et al. Transfer Printing of Metal Nanoparticles with Controllable Dimensions, Placement, and Reproducible Surface-Enhanced Raman Scattering Effects. *Langmuir* **2009**, *25* (8), 4347–4351.
- (18) De Silva Indrasekara, A. S.; Johnson, S. F.; Odion, R. A.; et al. Manipulation of the Geometry and Modulation of the Optical Response of Surfactant-Free Gold Nanostars: A Systematic Bottom-Up Synthesis. *ACS Omega* **2018**, *3* (2), 2202–2210.
- (19) Thomas, S.; Maiti, N.; Mukherjee, T.; et al. Investigation on the adsorption characteristics of anserine on the surface of colloidal silver nanoparticles. *Spectrochim. Acta, Part A* **2013**, *112*, 27–32.
- (20) Liu, Y.; Chao, K.; Nou, X.; et al. Feasibility of colloidal silver SERS for rapid bacterial screening. *Sens. Instrumen. Food Qual. Saf.* **2009**, *3* (2), 100–107.
- (21) Maruyama, Y.; Mitsuru, I.; Masayuki, F. Surface-Enhanced Raman Scattering of Single Adenine Molecules on Silver Colloidal Particles. *Chem. Lett.* **2001**, *30* (8), 834–835.
- (22) Basu, S.; Jana, S.; Pande, S.; et al. Interaction of DNA bases with silver nanoparticles: Assembly quantified through SPRs and SERS. *J. Colloid Interface Sci.* **2008**, *321* (2), 288–293.
- (23) Kneipp, H.; Kneipp, J.; Kneipp, K. Surface-Enhanced Raman Optical Activity on Adenine in Silver Colloidal Solution. *Anal. Chem.* **2006**, *78* (4), 1363–1366, DOI: 10.1021/ac0516382.
- (24) Kleinman, S. L.; Frontiera, R. R.; Henry, A. I.; et al. Creating, characterizing, and controlling chemistry with SERS hot spots. *Phys. Chem. Chem. Phys.* **2013**, *15* (1), 21–36.
- (25) Šimáková, P.; Procházka, M.; Kočíšová, E. SERS Microspectroscopy of Biomolecules on Dried Ag Colloidal Drops. *J. Spectrosc.* **2012**, *27*, No. 393847, DOI: 10.1155/2012/393847.
- (26) Šimáková, P.; Kočíšová, E.; Procházka, M. Sensitive Raman spectroscopy of lipids based on drop deposition using DCDR and SERS. *J. Raman Spectrosc.* **2013**, *44* (11), 1479–1482.
- (27) Hajduková, N.; Procházka, M.; Molnár, P.; et al. SERS of free-base porphyrins on immobilized metal gold and silver nanoparticles. *Vib. Spectrosc.* **2008**, *48* (1), 142–147.
- (28) Wassner, C.; Bradley, N.; Lee, Y. A Review and Clinical Understanding of Tenofovir: Tenofovir Disoproxil Fumarate versus Tenofovir Alafenamide. *J. Int. Assoc. Provid. AIDS Care* **2020**, *19*, No. 232595822091923.
- (29) Panel on Antiretroviral Guidelines for Adults and Adolescents. *Guidelines for the Use of Antiretroviral Agents in Adults and Adolescents with HIV*, 2023.
- (30) Venter, W. D. F.; Clayden, P.; Serenata, C. The ADVANCE study: a groundbreaking trial to evaluate a candidate universal antiretroviral regimen. *Curr. Opin. HIV AIDS* **2017**, *12* (4), 351–354.
- (31) Muller, J. T.; Al Khalili, Y. *Emtricitabine*, in *StatPearls [Internet]*; StatPearls Publishing, 2022.
- (32) Tantibanchachai, C. *FDA Approves First Injectable Treatment for HIV Pre-Exposure Prevention*; U.S. Food and Drug Administration, 2021.

(33) Brooks, K. M.; Anderson, P. L. Pharmacologic-Based Methods of Adherence Assessment in HIV Prevention. *Clin. Pharmacol. Ther.* **2018**, *104* (6), 1056–1059.

(34) McCluskey, S. M.; Govender, K.; Adamson, J.; et al. Point-of-care urine tenofovir testing to predict HIV drug resistance among individuals with virologic failure. *AIDS* **2023**, *37* (7), 1109–1113.

(35) Hermans, L. E.; Umunnakwe, C. N.; Lalla-Edward, S. T.; et al. Point-of-Care Tenofovir Urine Testing for the Prediction of Treatment Failure and Drug Resistance During Initial Treatment for Human Immunodeficiency Virus Type 1 (HIV-1) Infection. *Clin. Infect. Dis.* **2023**, *76* (3), e553–e560.

(36) Abaasa, A.; Hendrix, C.; Gandhi, M.; et al. Utility of Different Adherence Measures for PrEP: Patterns and Incremental Value. *Aids Behav.* **2018**, *22* (4), 1165–1173.

(37) Butler, M. R.; Hrnčirova, J.; Jacot, T. A. et al., Detection and quantification of antiviral drug tenofovir using silver nanoparticles and surface enhanced Raman spectroscopy (SERS) with spatially resolved hotspot selection. *Front. Nanotechnol.* **2023**, 51270474.

(38) Blank, P. S.; Sjomeling, C. M.; Backlund, P. S.; et al. Use of cumulative distribution functions to characterize mass spectra of intact proteins. *J. Am. Soc. Mass Spectrom.* **2002**, *13* (1), 40–46.

(39) Markello, T. C.; Carlson-Donohoe, H.; Sincan, M.; et al. Sensitive quantification of mosaicism using high density SNP arrays and the cumulative distribution function. *Mol. Genet. Metab.* **2012**, *105* (4), 665–671.

(40) Leopold, N.; Lendl, B. A New Method for Fast Preparation of Highly Surface-Enhanced Raman Scattering (SERS) Active Silver Colloids at Room Temperature by Reduction of Silver Nitrate with Hydroxylamine Hydrochloride. *J. Phys. Chem. B* **2003**, *107* (24), 5723–5727.

(41) Kent Lawson Wise, J. B. C.; Christian Lee Schoen Dispersive Near-IR Raman Spectrometer. In *PatFT*; USPTO, Ed.; Micron Optical Systems: United States, 2002.